Pis'ma v ZhETF, vol. 93, iss. 6, pp. 331 – 336

The LPM air showers initiated by UHE neutrinos and their detection by the satellite-based experiment

K. Miyazawa, K. Higashide, I. Nakamura, M. Kato[+], *A. Misaki*[∇], *H. P. Vankov*[*], *N. Inoue*

The Graduate School of Science and Engineering, Saitama University, 338-8570 Saitama, Japan

[+] *Kyowa Interface Science Co., Ltd., 351-0033 Saitama, Japan*

[∇] *Advanced Research Institute for Science and Engineering, Waseda University, 169-0092 Tokyo, Japan*

[*] *The Institute for Nuclear Research and Nuclear Energy, Bulgarian Academy of Sciences, BG-1784 Sofia, Bulgaria*

Submitted 25 January 2011

The Ultra-High-Energy(UHE) atmospheric showers with strong influence of the Landau-Pomeranchuk-Migdal(LPM) effect (here after LPM-showers) are exclusively expected to be produced by UHE neutrinos. Studies on the characteristics of the LPM-showers are essentially important to discriminate neutrino-shower (which produced by neutrino interaction) from hadronic shower (initiated by primary hadron). We calculate the LPM-showers initiated by electrons with energies of 10^{18} eV to 10^{21} eV, using the hybrid method as exactly as possible. Reflecting the change in the air density along the shower trajectories, the variety of the LPM-shower profiles is shown in different cases for their starting points in atmosphere. Through the study of time profiles of air fluorescent photon components from the LPM-showers, the detection capability of UHE neutrinos has also been investigated by the satellite-based experiment with a large acceptance, e.g., the TUS experiment.

1. Introduction. The composition of UHE cosmic rays with energies $> 10^{19}$ eV is one of unsolved questions, and its study will provide us the fruitful information on the origin and the acceleration mechanism of UHE cosmic rays. Especially, the detection of UHE neutrinos will be a key to solve these questions. Cosmogenic neutrinos have been expected to be produced in the interactions of UHE protons with cosmic background photons [1, 2]. The possibility of neutrino production during the particle acceleration in an Active Galactic Nuclei or a Gamma Ray Burst has also been pointed out [3]. Futhermore, UHE neutrinos could be expected in the top-down scenarios like the decay of Super Heavy Relic/Topological Defects [4, 5]. Despite their very small interaction cross-section, neutrinos interact with nucleons and create Extensive Air Showers(EAS) that receive the energy from the 80% of neutrino energy at an average. UHE neutrinos can be detected by produced EAS observation. Neutrinos create showers deep in the atmosphere, mostly largely inclined or horizontal showers, or even upward-going showers. The atmospheric depth at the EAS maximum ($X_{\max}$ in g/cm^2) can be used to distinguish neutrino showers from those of primary protons or nuclei.

It is well known that the LPM effect is stronger in high density materials, such as lead and iron [6 – 8]. However, for very high energies the LPM effect could be effective even in lower density materials, such as air. In the atmosphere the LPM effect becomes significant at energies $> 10^{16}$ eV, suppressing the Bethe-Heitler (BH) cross sections for bremsstrahlung and pair production [9]. The electromagnetic showers, affected by the LPM effect, are too different from the BH showers. Their average behavior shows significant elongation compared to the BH showers [10 – 14] and the individual LPM-shower profile sometimes shows multi-peak structure over wider slant depth [15].

Due to their very low interaction probability, from the high detection capability of the LPM-showers initiated by UHE neutrinos, a huge amount of target mass is required to assuring the interactions in atmosphere. The planned experiments TUS [16] and JEM-EUSO [17] are the suitable opportunity to observe UHE neutrino showers. Both experiments will detect the fluorescent light from the EAS by telescopes placed on satellites and have a large field of view (FOV) with a radius of 40 and 250 km, respectively. The target masses are 0.06 and one tera-ton, respectively.

2. The characteristics of the LPM Shower profiles. The largely inclined and horizontal showers, initiated by electrons have been simulated to study their time and longitudinal profiles. The LPM-showers traversing the atmosphere horizontally at different altitudes and the observation from the satellite telescope are schematically shown in Fig.1.

The shower development was followed by direct Monte Carlo simulation that includes the LPM effect down to threshold energy 10^{16} eV. The subthreshold par-

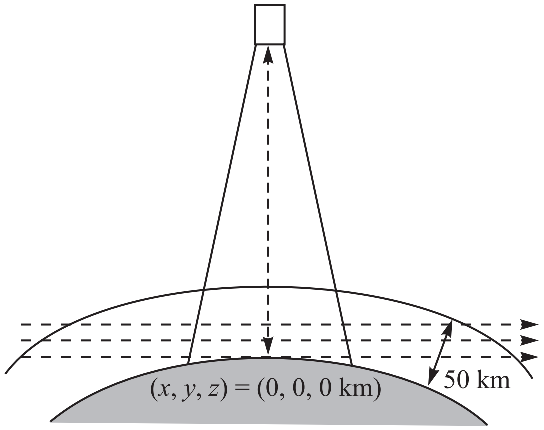

Fig.1. Schematic view of LPM-showers traversing the atmosphere without colliding with the Earth

ticles are replaced by analytical approximation of shower profile – NKG function [18].

To illustrate the impact of the LPM effect on the electromagnetic processes, in Fig.2, the differential cross sections for bremsstrahlung at the depth of 100 g/cm^2 in the atmosphere are shown (top of the figure). The LPM suppression above 10^{19} eV is clearly seen compared with the Bethe-Heither cross section. As the LPM effect is a kind of density effect, it becomes much stronger as more dense atmospheric layers.

The mean free path of the electron for the bremsstrahlung process as a function of the electron energy at the each depth (1–1000 g/cm^2) is also shown in the Fig.2 (bottom).

Therefore, the behavior of the LPM-shower is an important key feature of neutrino initiated shower. The average LPM-shower profiles with primary energy of 10^{20} eV, traversing the atmosphere horizontally at different heights of 0, 10 and 20 km, are shown in Fig.3. The starting points of each shower indicated by the distances from the FOV center (0,0,0) are defined: -70, -10 and -220 km, respectively. There is no descrepancy among average shower profiles at different heights in a unit of g/cm^2, but shower profiles developed in the region with smaller air density layers become wider than those developed in the larger air density when the distance is expressed in a unit of km.

In order to examine the influence of air density on the LPM-shower profile, we simulated horizontal LPM-showers of 10^{19}, 10^{20} and 10^{21} eV at a height of 10 km and different starting points of shower developments, i.e. 0 g/cm^2 (the outer edge of the atmospheric shell) and 2500 g/cm^2 from the outer edge, as shown in Fig.4. The LPM-showers starting at 0 g/cm^2 develop in smaller atmospheric density region, and their profiles show smooth

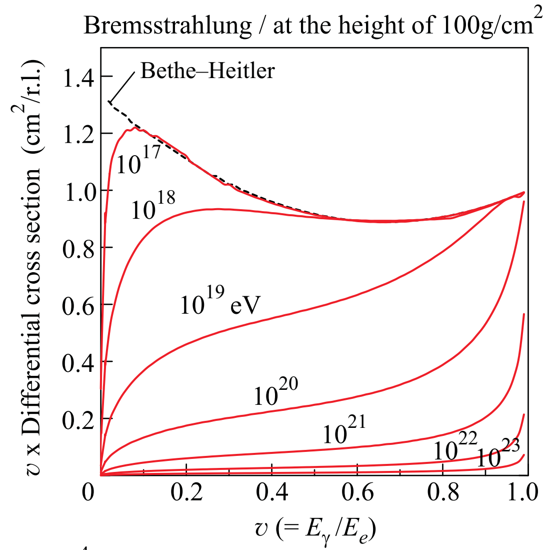

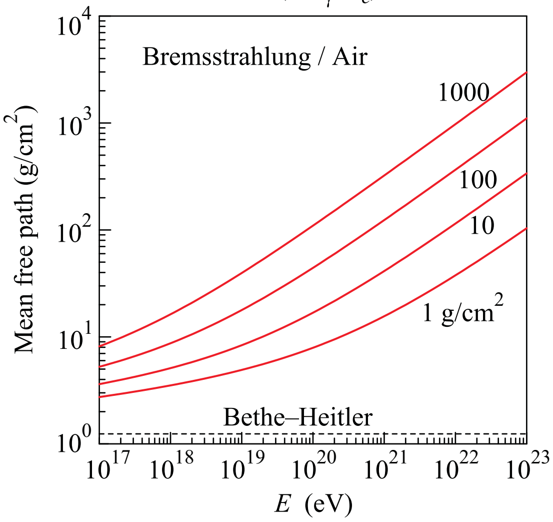

Fig.2. The differential cross sections for bremsstrahlung at the height of 100 g/cm^2 (top) and the mean free path for bremsstrahlung as a function of electron energy (bottom)

shapes and do not depend on the primary energy. On the other hand, showers starting at 2500 g/cm^2 and traversing dense air region, show profiles with larger fluctuations especially for energies above 10^{20} eV. Also it is easy to see that the profiles of EASs at the energy of 10^{21} eV show sometime multi-peak structures and variety of profile shapes.

The UHE LPM-showers traversing the atmosphere horizontally undergo large fluctuations which increase with the primary energy. Therefore the average characteristics of the LPM-showers are not so informative and we must analyze individual showers, especially in the highest energy region.

3. UHE neutrino showers. The UHE neutrino simulation code consists of the neutrino interaction

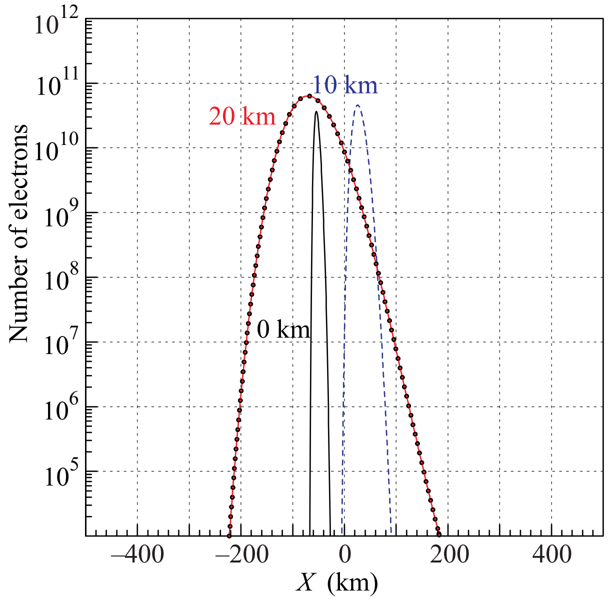

Fig.3. The horizontal LPM-shower profiles of 10^{20} eV, traversing at heights of 0, 10 and 20 km. The starting points of each shower are assumed as $x = -70$, -10 and -220 km

process, the EAS generation and the production of air fluorescent and Cherenkov photons in its development. The interaction cross-section with the atmospheric nucleus $\sigma_{cc}(\nu N)$ [cm^2] as a function of neutrino energy is given by eq. (1) [19]. The interaction length L_{int} [g/cm^2]of UHE neutrino related to the cross-section in atmosphere is expressed by eq.(2):

$$\sigma_{cc}(\nu N) = 5.53 \times 10^{-36}(E_\nu/1GeV)^{0.363}, \qquad (1)$$

$$L_{\rm int} = 1/(\sigma_{cc}(\nu N) \cdot N_A), \qquad (2)$$

N_A and E_ν are the Avogadro's number and the neutrino energy.

The US standard atmospheric model [20] is used to estimate the air density ρ [g/cm^3] as a function of the vertical height. The neutrino shower is generated by the secondary electrons produced in the neutrino interaction and the ratio between the EAS energy(E_e) and initial energy(E_ν) [21] is given by

$$E_e/E_\nu = (0.6724 + 0.0058 \log E_\nu). \qquad (3)$$

Electro-magnetic EASs have been generated by our own code as described in previous chapter. The individual longitudinal profiles are fitted by the Gaisser-Hillas formula [22], and they are accumulated in the database of EAS longitudinal profiles.

The $L_{\rm int}$ in atmosphere for energies of 10^{19}, $10^{19.5}$ and 10^{20} eV are $7.0 \cdot 10^7$, $4.6 \cdot 10^7$ and $3.0 \cdot 10^7$ g/cm^2,

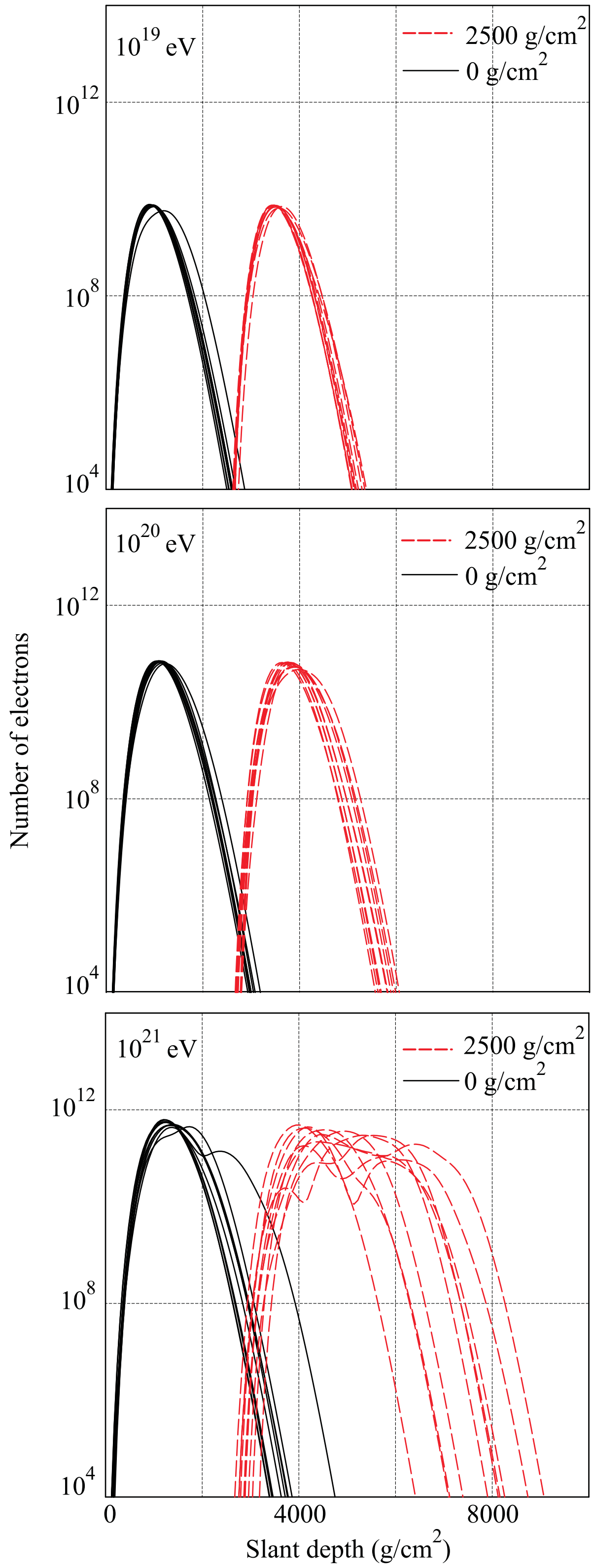

Fig.4. The individual horizontal LPM-shower profile of 10^{19}, 10^{20} and 10^{21} eV for different air densities at a height of 10 km. Starting points of LPM-showers set to 0 and 2500 g/cm^2

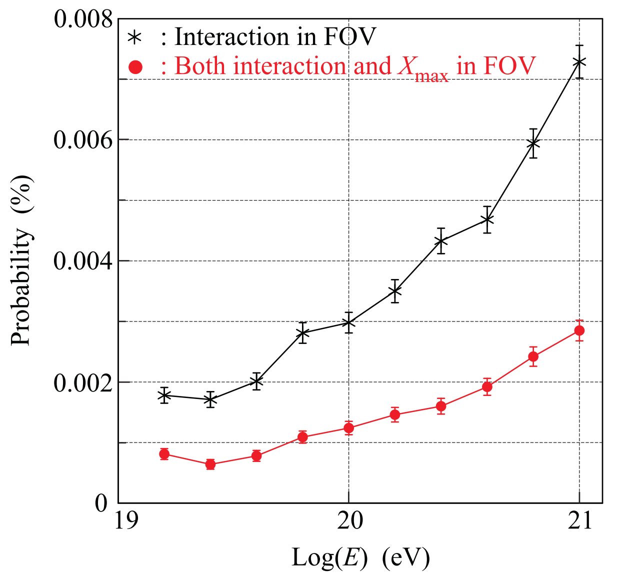

Fig.5. The interaction probability of UHE neutrinos in TUS's FOV as a function of neutrino energy is shown by star symbol. The probability in a case that both interaction and $X_{\max}$ is contained in a FOV, is shown by closed circle

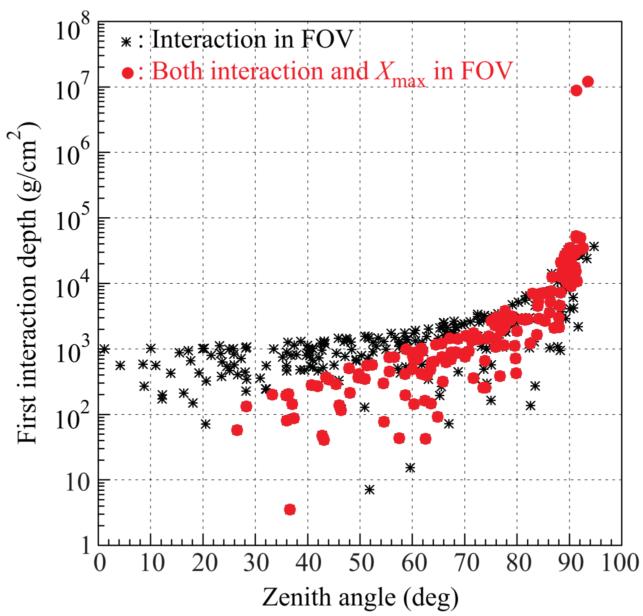

Fig.6. The relation between the first interaction depth and the incident zenith angle for neutrinos with energies of 10^{20} eV is shown by star symbols. The relation in a case that both interaction and $X_{\max}$ is contained in a FOV, is shown by closed circles

respectively. Therefore, the distribution of first interaction depth in 0–72000 g/cm^2 (a maximum slant depth for the horizontal incident at a height of 0 km) is almost uniform while the corresponding distribution for the hadronic cosmic rays is hardly exceeding 1400 g/cm^2 with a probability of $3 \cdot 10^{-6}$ because of the shorter interaction mean free path < 100 g/cm^2.

The interaction probability of UHE neutrinos in an atmospheric volume defined by a FOV of the satellite EAS telescope is shown in Fig.5, as a function of the energy. The target atmospheric mass is just assumed as the acceptance of TUS experiment with a FOV of $\pm 4.5°$ from the height of 550 km in this calculation. 10^7 neutrinos for each energy between $10^{19.2}$ and 10^{21} eV are injected to a FOV with zenith angles between 0° and 95° sampled from the zenith angle distribution following a sine function. The interaction probability which indicates the ratio between the number of interacted neutrinos and all incident ones, is nearly 0.003% at the energy of 10^{20} eV and it increases with energy. In the figure, the probability in a case that both interaction and $X_{\max}$ is fully contained in a FOV, is shown by closed circle, and it gives 0.0012% at energy of 10^{20} eV.

Fig.6 shows the relation between the first interaction depth in a FOV and the incident zenith angle. 10^7 neutrinos with energies of 10^{20} eV are injected with same zenith angles distribution into a TUS's FOV. EASs initiated by neutrinos with larger zenith angles, typically $> 70°$, can be observed dominantly because the larger slant depth of atmosphere has a larger chance probability to produce EAS. Events appeared at $1 \cdot 10^7$ g/cm^2 are the ground-skimmed events initiated by neutrinos with zenith angles between 90° and 95°.

4. The detection of UHE neutrino shower. The neutrino EAS is generated at the first interaction point where is determined by the assumed interaction mean free path. The detection capability of UHE neutrino EAS by the satellite-based telescope is examined in this study, therefore, the emission of air fluorescent and Cherenkov photons from EAS particles are also calculated in our code. The fluorescent photon yield [23] in a unit of photons/(m·electron) is applied for photon production at 10 g/cm^2 intervals along the shower development. The Rayleigh scattering of photons in atmosphere is also taken into account in their propagations.

The number of arrival photons at the TUS telescope is estimated with the known features, (i) the optical mirror size of 1.8 m in a diameter, (ii) the observation from the height of 550 km with a FOV of $\pm 4.5°$, (iii) the Time-Resolution-Unit(TRU) of 0.8 μs and the size of ground segment of 5.5 km. Fig.7 indicates the arrival photon profiles at the telescope initiated by the same horizon-

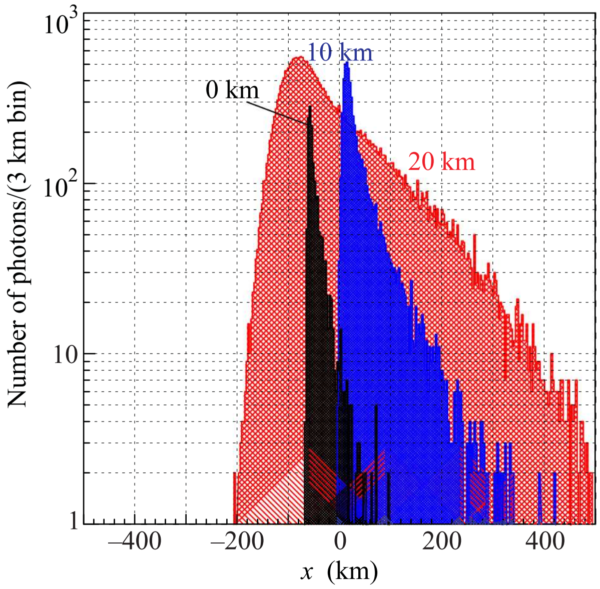

Fig.7. Expected fluorescent photon profiles by the telescope, calculated from shower profiles in Fig.3

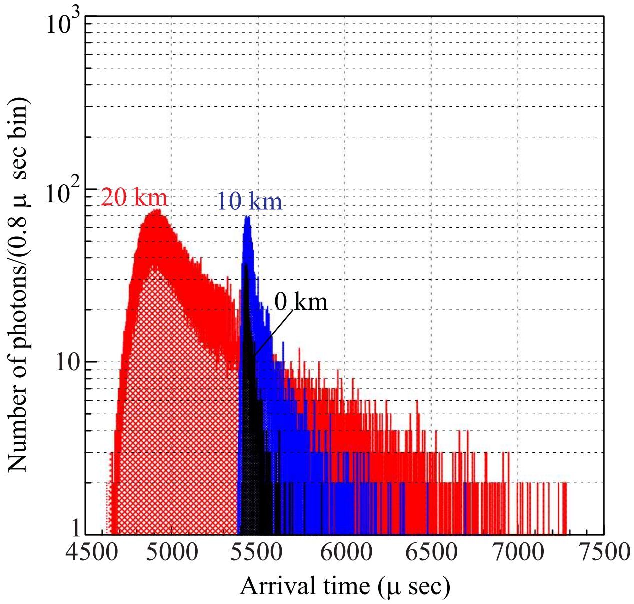

Fig.8. The time profiles of arrival photons of neutrino EASs with the energy of 10^{20} eV and the zenith angle of 90°. EASs passing through at the different altitudes of 0, 10 and 20 km

tal LPM-showers shown in Fig.3. The EAS developed in a lower air density at a higher atmosphere, produces a larger number of photons than that in the lower atmosphere, because the fluorescent photon yield in a unit of photons/(m·electron) does not depend so much on the height between 0 km and 20 km. In addition to the fluorescent photons, longer tails can be found in the profiles, as a contribution of the scattered Cherenkov photons. The time profiles of arrival photons at the telescope are shown for horizontal EASs with an energy of 10^{20} eV passing through at the different heights of 0, 10 and 20 km in Fig.8. The numbers of photons binned in every 0.8 μs are plotted.

In order to estimate the detection capability of neutrino EASs by the TUS, following assumptions and procedures have been taken into account, (i) The 3 different neutrino energy spectra (a) $\phi = 1.7 \cdot 10^{11} \times E^{-2.5}$, (b) $\phi = 5.4 \cdot 10^{10} \times E^{-2.5}$ and (c) $\phi = 5.4 \cdot 10^{20} \times E^{-3}$ are assumed as shown in Fig.9, (ii) 5 $\cdot 10^6$ neutrinos are injected with energies sampled from each energy spectrum, (iii) After confirming the interaction in a FOV, EAS initiated by neutrino is generated in atmosphere and the characteristics of arrival photons at the telescope; the arrival time, the wave length and the emission point (x, y, z), are recorded as the output data, (iv) The judgement on event trigger is done by satisfying the condition of 5 successive TRUs with >35 photons in each TRU. This required photon number in a TRU corresponds to a level of 3σ higher than the average background photons of 500 photons/(m^2·sr·ns) assumed in this calculation. The expected numbers of neu-

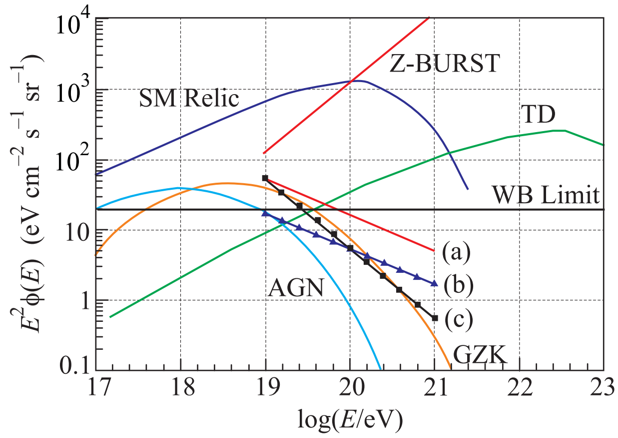

Fig.9. 3 different energy spectra used in the simulation are plotted by the lines of (a), (b) and (c). Neutrino fluxes per flavour: AGN from Mannheim, 1995 [24]; GZK from Protheroe and Johnson, 1995 [25]; TD from Sigl et al., 1997 [26]; SM Relic particle from Kalashev et al., 1999 [27]; Z-BURST from Kalashev et al., 2002 [28]; The intensity of the Waxman-Bahcall limit [29] is shown with a horizontal black line in the figure

trino EASs with $>10^{19.9}$ eV are $5.6\cdot10^{-3}$, $1.8\cdot10^{-3}$ and $1.4 \cdot 10^{-3}$ events/year for the energy spectra of (a), (b) and (c), respectively.

5. Conclusion. The LPM-showers are expected to be produced by UHE neutrinos, and their average and individual profiles have been studied to estimate for the detection capability of UHE neutrinos by the satellite-based observation, e.g. the TUS experiment. Actually, the LPM effect is a kind of density effect, and it becomes stronger in the denser atmosphere and typically in an energy region $>10^{20}$ eV. The LPM-showers initiated by UHE neutrinos with largely inclined and energies $>10^{20}$ eV undergo large fluctuations, which show sometime multi-peak structures as a variety of LPM-shower profile shapes. This is an advantageous characteristics when the candidate for neutrino EAS is identified from the pool of hadronic EAS. In addition, the observation of Xmax is most powerful key to discriminate neutrino EAS. The Xmax distribution of neutrino EASs is almost uniform over the cumulative atmospheric depth of 72000 g/cm^2 while one for the hadronic EASs is not exceeding 1400 g/cm^2 with a probability of $3\cdot10^{-6}$ because of its shorter interaction mean free path. Therefore, the detection of UHE neutrinos is expected through the observation of EAS profiles by the satellite-based air fluorescent telescope with a large acceptance and target mass. The expected numbers of neutrino EASs with $>10^{19.9}$ eV could be $7.0\cdot10^{-3}$–$2.8\cdot10^{-2}$ events for 5 years TUS observation with assumptions of neutrino energy spectra. This is not enough detection capability with a present spec of the TUS experiment, however the TUS telescope has a cumulative exposure of $3\cdot10^{4}$ km^2 sr year in 5 years observation which is equivalent to the one by a 5 years AUGER experiment. The detection capability of UHE neutrinos is strongly dependent on the neutrino flux and few statistics will be expected even in an optimistic case. The TUS experiment has still potential to detect UHE neutrinos with the best reliability as the first EAS observation from the satellite.

H. Vankov wants to JSPS for its support to work in the Saitama University.

---

1. K. Greisen, Phys. Rev. Lett. **16**, 748 (1966).
2. G. T. Zatsepin and V. A. Kuzumin, Pis'ma v Zh. Eksp. Theor. Fiz, **4**, 144 (1966).
3. A. Cuoco and S. Hannestad, arXiv:0712.1830v2 [astro-ph].
4. P. Bhattacharjee, C. T. Hill, and D. N. Schramm, Phys. Rev. Lett. **69**, 567 (1992).
5. V. Berezinsky and A. Vilenkin, Phys. Rev. Lett. **79**, 5202 (1997).
6. L. D. Landau and I. J. Pomeranchuk, Dok. Akad. Nauk. SSSR **92**, 535 (1953).
7. L. D. Landau and I. J. Pomeranchuk, Dok. Akad. Nauk. SSSR **93** 735 (1953).
8. A. Migdal, Phys. Rev. **103**, 1811 (1956).
9. H. A. Bethe & W. Heitler, Proc. Roy. Soc. **164**, 257 (1936).
10. E. Konishi, A. Misaki, and N. Fujimaki, Il Nuovo Cim. A **44**, 509 (1978).
11. T. Stanev, Ch. Vankov, R. E. Streitmatter et al., Phys. Rev. D **25**, 1291 (1982).
12. A. Misaki, Phys. Rev. D **40**, 3086 (1990).
13. A. Misaki, Il Nuovo Cim. C **13**, 733 (1990).
14. A. Misaki, Fort. Schritt. d. Physik. **38**, 413 (1990).
15. E. Konishi, A. Adachi, N. Takahashi, and A. Misaki, Jour. Phys. G **17**, 719 (1991).
16. V. Abrashkin, V. Alexandrov, Y. Arakcheev et al., Adv. in Space Research **37**, 1876 (2006).
17. T. Ebisuzaki et al., Nucl. Physics B (Proc. Suppl.) **175-176**, 237 (2008).
18. K. Greisen, Progress in Cosmic Ray Physics. North-Holland **1** Vol.3 (1956).
19. R. Gandhi, C. Quigg, M. H. Reno, and I. Sarcevic, Phys. Rev. D **58**, 093009 (1998).
20. U.S. Standard, Atmosphere, U.S. Government Printing Office, Washington, D.C. (1976).
21. R. Gandhi, C. Quigg, M. H. Reno, and I. Sarcevic, Astropart. Phys. **5**, 81 (1996).
22. T. K. Gaisser and A. M. Hillas, Proc 15th ICRC (Plovdiv), **8**, 353 (1977).
23. M. Nagano, K. Kobayakawa, N. Sakaki, and K. Ando, Astroparticle Physics **22**, 235 (2004).
24. K. Mannheim, Astroparticle Physics **3**, 295 (1995).
25. R. J. Protheroe and P. A. Johnson, Astroparticle Physics **4**, 253 (1995).
26. G. Sigl, S. Lee, D. N. Schramm, and P. Coppi, Phys. Lett. B **392**, 129 (1997).
27. O. E. Kalashev, V. A. Kuzmin, and D. V. Semikoz, arXiv:9911035v3[astro-ph] (1999).
28. O. E. Kalashev, V. A. Kuzmin, D. V. Semikoz, and G. Sigl, arXiv:0205050v3[hep-ph] (2002).
29. E. Waxman and J. Bahcall, Phys. Rev. D **59**, 023002 (1998).